Pt-CoOx nanoparticles supported on ETS-10 for preferential oxidation of CO reaction

Angela López, Nuria Navascues, Reyes Mallada*, Silvia Irusta*

Nanoscience Institute of Aragon and Chemical and Environmental Engineering Department, University of Zaragoza, 50018 Zaragoza, Spain

*Corresponding authors

Abstract

In this paper we prepare bimetallic Pt-CoOx nanoparticles which are further supported in microporous titanosilicate ETS-10. This support has been previously demonstrated as a good candidate for this reaction in the presence of CO_2 and H_2O. The bimetallic nanoparticles and the supported catalysts containing different loadings of nanoparticles have been extensively characterized and tested in the PROX reaction. The characterization of the nanoparticles discarded the formation of a metallic alloy, although Co and Pt are intimately in contact in the nanoparticle as the HAADF-STEM images revealed. XPS confirmed that the calcined nanoparticles would consist of metallic platinum and cobalt and Pt oxides. The catalyst containing 1.4 wt.% of PtCo nanoparticles can achieve complete CO conversion in the temperature range 120-150ºC working at WHSV=30 L h^{-1} g^{-1}.

Key words: Bimetallic catalyst, PtCo nanoparticles, PROX, ETS-10

1. Introduction

Among the many approaches to reduce CO concentration in the reformed gas mixture to the levels required for the use in low temperature Proton Exchange Membranes Fuel Cell (PEMFC), preferential catalytic oxidation of CO to CO_2 (PROX) has been considered as the most promising [1]. An efficient catalyst for this reaction should convert CO avoiding the competing oxidation of H_2. In fact, such an ideal catalyst should convert CO molecules in the presence of a large excess of H_2, together with other components that can negatively affect the activity, like H_2O or CO_2 [2]. Typical reformate gas compositions at the exit of the water gas shift reactor include 15–20 vol.% CO_2, 0.5–2 vol.% CO and about 15–25 vol.% H_2O and H_2 in high concentrations [3]. Due to the presence of these molecules in the reactor feed, the influence of H_2O and CO_2 on Pt group catalysts on different supports has been studied. On Pt-Co catalysts supported on alumina it was found that the presence of water showed a positive effect on CO conversion but only below 120ºC [4]. When aluminumphosphates were used as support a slight negative effect of CO_2 on CO conversion was ascribed to the adsorption on the active sites for activating oxygen. In this case water also was found to have a negative effect on CO conversion probably because of the adsorption on the support [5]. Since the discovery of ETS-10 and ETS-4 by Kuznicki [6] these titanosilicates have attracted increasing interest and they have been studied extensively. In particular ETS-10 presents high capacity ion exchange isomorphic substitution and low acidity. We have previously studied the effect of water and CO_2 on Pt–ETS-10 catalysts[3] and a strong inhibition on CO conversion was observed after the introduction of CO_2. This was explained by taking into account the basic nature of ETS-10 that gives rise to a strong interaction with CO_2, a reactant of acid nature. However, in the presence of water this effect was completely reversed. The water favored the formation of surface OH groups, which enhanced the Brønsted acidity of ETS-10 and compensates the strong inhibition

effect of CO_2. These observations make ETS-10 a good candidate as support for PROX reaction in the presence of water and CO_2.

It is known that Pt catalysts are excellent for hydrogen oxidation, but in the presence of CO it is inhibited due to the strong CO adsorption and high CO coverage hindering the available sites for hydrogen and oxygen adsorption and further dissociation [7]. With increasing temperature the CO coverage decreases and the hydrogen oxidation starts competing for oxygen. The modification of the surface electronic structure and chemical properties on Pt, by the introduction of other subsurface 3d transition metals, was theoretically demonstrated at the beginning of this century by Kitchin et al.[8]. Since then the preparation and study of Pt bimetallic catalyst has grown exponentially and several reviews have been published in this field recently [9, 10]. To enhance the activity in the PROX reaction several non-noble metals have been added to the Pt catalysts such as Co, Ni, Cu, Fe, Mn, Sn [1], which clearly increase the activity of platinum in this reaction, among them Co and Fe seem to be the most promising.

The addition of cobalt to Pt nanoparticles on different supports was found to improve the catalytic activity for the PROX of CO [4, 5, 11-16]. However only some of the catalysts were tested under simulated reformate streams containing all the components [4, 5, 11, 15]. There is a debate about the active phase in these catalysts for PROX. The group of Komatsu claimed that the active phase corresponds to the Pt_3Co intermetallic compound [11, 17]. On the contrary Xu et al. proposed an architecture of the Pt-Co bimetallic catalyst consisting of Pt nanoparticles decorated with highly dispersed CoO nanostructures [18].

The reported Pt-Co catalysts tested in the PROX reaction were prepared by simultaneous or successive impregnation of precursor salts on the support followed by thermal treatments [4, 5, 10, 11, 13, 15]. By employing recent methods, developed in the field of nanotechnology for the synthesis of colloidal suspensions of metallic nanoparticles, Pt-Co nanoparticles can be

synthesized in a controlled manner as preformed nanocatalysts before they are applied on support materials. This approach has been followed by several authors for different reactions such as Fischer-Tropsch [19], methanol oxidation reaction [20], CO_2 hydrogenation [21] and selective carbonyl reduction in α,β-unsaturated aldehydes [22]. However, to the best of our knowledge, this strategy has not been pursued for the preparation of bimetallic Pt-Co catalysts tested in PROX reaction.

In this work Pt-Co nanoparticles were synthesized in solution and afterwards supported on microporous titanosilicate ETS-10. The materials were characterized by SEM, TEM, XRD, XPS and tested in PROX in a stream containing carbon dioxide and water besides a high concentration of hydrogen. The goal is to develop a two-step preparation method for controlling the synthesis of the bimetallic active phase, followed by deposition in an appropriate support. Furthermore we will get insight into the catalytic active phase thanks to the characterization of the bimetallic nanoparticles and the catalytic activity tests for different nanoparticle loadings and reaction conditions.

2. Materials and methods

2.1. *Nanoparticles synthesis*

The synthesis of the nanoparticles was divided in two successive reduction steps for Co and Pt salts, using $NaBH_4$ as reducing agent. The synthesis was performed at 0ºC under N_2 atmosphere to avoid any oxidation. This procedure is based on a synthesis protocol previously reported by Du et al [23]. In a typical synthesis 0.5g of PVP (MW=10000, Sigma-Aldrich) were dissolved in 100 mL of ethanolic solution 3.6 mM in $CoCl_2$ (Sigma-Aldrich, anhydrous, purity ≥98%). Then 100 mL ethanol solution 1.35 mM in $NaBH_4$ (Fluka. purity ≥99%) was added dropwise. The mixture color changes from blue to brown indicating the formation of metallic cobalt nanoparticles. After that, 100 mL of 10.8 mM H_2PtCl_6 (Sigma-Aldrich. purity ≥99%) ethanol solution was added and the resultant mixture was stirred for 30 minutes. Finally the Pt

was reduced adding 100 mL of 8.1 mM $NaBH_4$ (Fluka. purity ≥99%) ethanol solution dropwise. The mixture was kept under stirring for 3 hours at 0°C and finally ethanol was evaporated at 85°C. Part of the synthetized nanoparticles were calcined 3 h at 500ºC before characterization analysis.

2.2. Supported PtCo nanoparticles on ETS-10

The ETS-10 support was synthesized using anatase as titanium source according to the procedure previously described [24]. The molar gel composition corresponds to $4.4Na_2O:1.4K_2O:TiO_2:5.5\ SiO_2:125\ H_2O$. The gel was prepared dissolving NaCl (Merck, purity ≥99%) and KCl (Merck, purity 99.5%) in deionized water under stirring. Then sodium silicate (Merck 28.5% SiO_2 ; 8.5% Na_2O) was added slowly to the solution. After stirring for 3 hours, KF (Merck, purity 98.5%) and TiO_2 anatase (Sigma-Aldrich, purity ≥99.7%) were added. The solution was kept under stirring for one hour. The pH was adjusted to 10.4 using HCl to avoid impurities such as ETS-4 and AM-3 [25]. The obtained gel was introduced in an autoclave at 230ºC for 24h. After that the solids were recovered by filtration, washed with deionized water and dried at 100ºC.

The synthesized PtCo nanoparticles were incorporated to the support by incipient wetness impregnation method. The synthetized nanoparticles were dispersed in a volume of water enough to fill the porous of the support and put in contact with the ETS-10. The prepared catalysts are hereafter named as xNP/ETS, where “x” denotes the nanoparticles loading in wt%.

2.3. Characterization

The morphology, composition and particle size of nanoparticles, support and catalysts were characterized by Scanning Electron Microscope, SEM coupled with EDX detector, (FEI InspectF50) and Transmission Electron Microscopy, TEM, (FEI Tecnai F30) operated at 300 kV.

For TEM observations the samples were dispersed in ethanol in an ultrasonic bath for 15 minutes and deposited on a carbon grid. X-ray diffraction patterns were obtained in a PANalytical Empyrean equipment in Brag Bentano configuration using CuKα radiation and equipped with a PIXcel^{1D} detector, to identify the crystalline phases.

The bulk chemical composition of digested samples was analyzed using microwave plasma atomic emission spectrometry (Agilent 4100 MP-AES). The solid samples were digested in aqua regia for 20 minutes in an autoclave heated at 200 ºC in a microwave oven (Ethos Plus, Mileston).

The X-ray photoelectron analysis (XPS) was performed with an Axis Ultra DLD (Kratos Tech.). The spectra were excited by the monochromatized AlKα source (1486.6 e.V) run at 15 kV and 10 mA. For the individual peak regions, pass energy of 20 eV was used. Survey spectrum was measured at 160 eV pass energy. Analyses of the peaks were performed with the CasaXPS software, using a weighted sum of Lorentzian and Gaussian components curves after background subtraction.

Catalytic activity tests

The activity measurements were carried out using fixed-bed reactor configuration in a quartz tube of 9 mm internal diameter. The reactor was loaded with 100 mg of catalyst and 200 mg of quartz, used as a diluent. The reaction temperature was measured with a thermocouple located in the center of the catalyst bed. The composition of the feed stream was: 1%CO, 1%O_2, 3%H_2O, 21%CO_2 and hydrogen balance. Prior to catalytic activity tests, the solids were heated at 5 ºC/min up to 500 ºC in air and kept at this temperature for 3 h. Then the catalyst was cooled down to room temperature under N_2 atmosphere.

Feed and products were analyzed by gas chromatography with a Varian CP-4900 Micro-GC equipped with two modules containing, molecular sieve and PPQ columns respectively and using helium as carrier gas. Under the analysis conditions the detection limit of CO was 5 ppm.

The CO conversion, oxygen conversion and the selectivity of the PROX reaction were calculated according to:

$$\text{CO conversion (\%)} = \frac{\text{FCO feed} - \text{FCO outlet}}{\text{FCO feed}} * 100$$

$$O_2 \text{ conversion(\%)} = \frac{\text{FO2 feed} - \text{FO2 outlet}}{\text{FO2 feed}} * 100$$

$$\text{Selectivity(\%)} = \frac{\text{FCO feed} - \text{FCO outlet}}{2*(\text{FO2 feed} - \text{FO2 outlet})} * 100$$

The conversion values were obtained after the reactor temperature was stable for at least 30 min and the values reported represent the average of 3 samples taken at the reactor exit. Calculate selectivity gives the percentage of oxygen moles consumed for CO oxidation. CH_4 was not detected in any of the experiments carried out. The mass balance was measured and was always in the range 98-102 at.%.

3. Results

3.1. Pt-Co nanoparticles characterization

Figure 1 shows the TEM images (a) and particle size histogram (b) of the synthesized nanoparticles. The particles have spherical shape with diameter distribution obtained by measuring 100 particles in different images of 3.2±0.6 nm. HAADF-STEM elemental mapping images clearly show that Pt and Co atoms are distributed throughout the whole particle (Figure 1 c). The coexistence of Pt and Co elements in the particles was further confirmed by the EDS analysis (Figure 1 d).

The bulk atomic Pt to Co ratio obtained by MP-AES analysis was 3.0±0.04. On the other hand, SEM-EDX and XPS gave values of 2.4 ±0.6 and 1.7±0.2 respectively. Due to the different surface sensitivity of both techniques and comparing with the bulk composition, these results suggest that most of the cobalt could be on the surface of the nanoparticles.

Figure 2 displays the XRD pattern of the calcined nanoparticles. The diffraction pattern exhibits peaks in the 20-120º range corresponding to the platinum cubic structure, Fm-3m (JCPDS 01-

080-3827). It was previously reported that the Pt_3Co alloy formation would shift the Pt peaks to higher angles due to the incorporation of Co into the cubic structure and the concomitant lattice contraction [11, 26, 27]. Since no shift was observed, the incorporation of Co to the platinum lattice can be ruled out, even when both elements coexist in the same particle according to STEM results and it is known that they could form a continuous series of solids solutions [28]. Considering that no diffraction peaks of cobalt or its oxides were detected in the synthesized particles, most of Co species are possibly either amorphous [29, 30] or with crystallite size smaller than the technique detection limit. The crystallite size of Pt was calculated through Debye Scherrer formula using the full width at half-maximun of the Pt(111) diffraction peak. The value obtained for the Pt crystallite was 2.2nm which is similar to the measured values by TEM for the nanoparticles, see Figure 1. The difference with TEM results could be because XRD reflects the crystal grain size rather than the actual particle morphology [31]. Beside the mentioned signals, peaks related to NaCl can be observed, these crystals would be formed from the synthesis salts since chlorides are use as metal precursors and the reduction agent is a sodium salt.

XPS analysis of the bimetallic particles revealed the presence of carbon, cobalt, platinum, oxygen, sodium and chlorine. The binding energies were referenced to the internal C 1s (284.9 eV) standard (Figue 1 SI). Since the size of the nanoparticles prevents the purification of samples by centrifugation, all the compounds that are not eliminated by calcination at 500ºC remain in the final product (i.e., NaCl also detected by XRD).

The Pt 4f XPS spectrum of the synthesized particles can be fitted by three pairs of doublets (Figure 3a). The branching ratio was kept at the statistical value. The binding energies of the first Pt $4f_{7/2}$ component was located at 71.1 eV assigned to metallic platinum [32]. By measuring the relative peak areas, the percentage of Pt^0 species in the nanoparticles is calculated to be 43%. The other Pt $4f_{7/2}$ components at 71.8 and 74.2 eV were ascribed to PtO and PtO_2 [33]. Figure 3b shows the Co 2p core level with multiple peaks due to the spin orbital

splitting and final state features (shake-up satellites) of the $3d^6$ and $3d^7\underline{L}$ lines electronic structure for Co^{3+} and Co^{2+} in different cobalt oxide modification [34]. The Co $2p_{3/2}$ region was fitted with two peaks at 779.7 and 781 eV that were assigned to Co^{2+} and Co^{3+} oxidation states respectively [35]. The broad and low intensity satellite structure is due to the overlapping of the two satellites, typical for the Co_3O_4 spinel. The measured atomic ratio Co^{2+}/Co^{3+} was 1.33, showing an excess of Co^{2+} (57 at.%). The presence of metallic or alloyed cobalt in the nanoparticles can be ruled out due to the absence of a signal at lower binding energy (778.5 eV) [32, 36]. Even when the bulk Pt/Co atomic ratio is 3, XPS gives no evidence of the presence of Pt_3Co phase. According to XPS results the calcined nanoparticles would consist of metallic platinum and cobalt and Pt oxides.

3.2 Supported CoPt-NPs on ETS-10

TEM images of PtCo/ETS-10 catalysts show the presence of well dispersed nanoparticles, with size in the 3 to 4 nm range, on the surface of the ETS-10 crystals (Figure 4). There is a small increase in the calculated mean particle size after deposition on the support, from 3.5±0.5 nm in the 0.35NP/ETS catalysts to 3.8±0.6 nm in 1.20NP/ETS solid and 4.0±0.7 nm 1.40NP/ETS. The surface of the calcined solids was analyzed by XPS (Figure 2a SI), besides the adventitious carbon, the ETS-10 components Si, Ti, O and the cations Na and K were detected. Analysis of Ti 2p spectrum (Figure 2b SI)reveals that the binding energy is characteristic of octahedrally coordinated Ti atoms in ETS-10 [24]. The presence of sodium would be associated not only to the support but to de Cl also detected on the surface of catalysts.

3.3 Catalytic activity

The influence of space velocity on the catalytic behavior of 1.4NP/ETS was studied. CO conversion and CO_2 selectivity are shown in Figure 5 as a function of the catalyst bed temperature at different WHSVs. This behavior was fully reproduced in subsequent cycles of temperature increasing/decreasing indicating that after 30 min under reaction stream the catalysts reached their stable condition. In all cases, as the reactor temperature increased, the

CO conversion increases, reaches a maximum at an optimum temperature and then decreases. It can be observed that the conversion curves shift to higher temperature with increasing the space velocity. At a WHSV of 120 L g^{-1} h^{-1}, this optimum temperature was 224 °C, corresponding to a CO conversion of 84%. As the WHSV decreased to 60 and then to 30 L g^{-1} h^{-1}, the optimum temperatures shifted to 174 and 125 C respectively, but in these cases the complete CO conversion was achieved. For the lower WHSV the 100% CO conversion was maintained in a 25 ºC operating window from 125 to 150ºC. As expected the selectivity for the highest conversions was around 50%.

The CO PROX performance of catalysts with different nanoparticles loading is compared in Figure 6. Working at WHSV= 30 L g^{-1} h^{-1} in all the solids 100% CO conversion was achieved. As expected the increase in the nanoparticles load from 0.35 wt% to 0.78 and 1.20 wt% shifted the CO conversion curve to lower temperatures. Further increase of the nanoparticles loading to 1.40wt% improves the catalytic behavior reaching the complete CO conversion at 125 ºC. The decrease in CO conversion at higher temperatures occurs due to oxygen scarcity caused by acceleration of undesirable concurrent hydrogen oxidation reaction mentioned before which results in a selectivity decrease [13]. It is important to notice that all the catalysts, except the 0.35NP/ETS exhibit 25ºC operating window where the concentration of CO is below the detection limit

The stability of 1.4NP/ETS catalyst was evaluated by continuous operation for 50 h at 75 ºC, with a WHSV of 30 L g^{-1} h^{-1}, the results are presented in Figure 7. A conversion level of around 30% with a selectivity of 70% was maintained for more than 50 hours, even in the presence of water and carbon dioxide.

4. Discussion

Pt-Co catalysts obtained by deposition of synthesized Pt-Co nanoparticles on ETS-10 with low platinum loading (1.4 wt%) achieve the complete CO conversion at 125 ºC, working at WHSV=

30 L g^{-1} h^{-1} in presence of water and CO_2. This activity was maintained for 50 h on reaction stream. In the literature there are works reporting the activity in the presence of H_2O and CO_2 of Pt-Co catalysts with low Pt loading. Ko et al. [16] reported a Pt-Co catalyst (0.5%Pt-Co/YSZ, Co/Pt=10) that maintains the concentration of CO in the outlet stream lower than 10 ppm of CO in the range of 100 to 150ºC % working at 16.7 L g^{-1} h^{-1} a much lower space velocity than the used in this work.

A solid with 1wt%Pt and 2wt% Co supported on cobalt modified AlPO-5 also presented total CO conversion in the range 110-125 ºC also at a WHSV slightly lower than the used in this work (24 L g^{-1} h^{-1}), besides the stability of the catalysts was not tested [5]. On the other hand, Yan et al. [4] worked at WHSV 40 L g^{-1} h^{-1}, higher than ours, in a catalyst with 1wt% Pt and 3 wt% Co supported on alumina obtaining 100% CO conversion at 120 ºC, in this case the stability was also no reported. Finally Wang et al. [11] reported complete removal of CO at temperatures ranging from 40 to 150ºC and 30 L g^{-1} h^{-1} with an optimized catalyst containing a load of Pt as high as 4% and 0.7%Co supported on carbon nanotubes. Summing up the activity results presented in this work, with preformed PtCo NPs supported on ETS-10 are among the best reported literature values.

Komatsu and Tamura [11] claim that the active species for PROX at low temperatures in Pt-Co supported on silica are Pt_3Co and PtCo. However, the catalysts loaded with 3wt% Pt, were tested in absence of water and carbon dioxide. Even when the bulk atomic ratio in the prepared nanoparticles was Pt/Co=3, no evidences of any intermetallic compound was found in our catalysts (XPS and XRD results) suggesting that Pt/CoO is the active specie in a typical reformate gas stream .On YSZ supported Pt-Co solids, the high activity was attributed to the presence of isolated Pt-Co nanoparticles interacting with the support [16]. Because of the good particles dispersion observed in TEM images, the good catalytic performance of 1.4NP/ETS could be associated to isolated Pt-Co nanoparticles. On the other hand, HAADF-STEM mapping

of particles confirm the presence of both Pt and Co in the same particle, these would favor the synergistic interaction between metallic Pt and CoO (XPS results) promoting the high CO-PROX performance of PtCoNP/ETS catalysts [12, 18]. Another interesting characteristic of our catalysts is the presence of Na, not only as exchange ion in the support, but also remaining from the synthesis process. It is known that sodium enhances the PROX activity of platinum-cobalt catalyst up to a sodium content of 2 wt% [37]. The effect of the sodium addition would be related to the promotion of oxygen adsorption on platinum, lowering the temperature regions in which carbon monoxide adsorption does not inhibit the adsorption of oxygen. The positive effect of sodium would be more important than the possible negative effect of chlorine blocking the sites which are able to activate the CO molecule that was found for Pt/ceria catalysts [38].

5. Conclusions

Pt-Co catalysts were obtained by deposition of synthesized Pt-Co nanoparticles consisting of metallic platinum and cobalt and Pt oxides (Pt/Co bulk atomic ratio=3) on ETS-10 support. The catalysts showed high activity for the selective oxidation of CO in a simulated reformate gas stream with high hydrogen concentration (74 vol%). The solid containing 1.4 wt% of nanoparticles can achieve complete CO conversion in the temperature range 120-150ºC working at WHSV=30 L $h^{-1}g^{-1}$. The stability of this solid was tested for 50 h, showing no changes in CO conversion or selectivity. The activity of the prepared catalysts would be related to the good dispersion of the nanoparticles on the support, the presence of CoO on the surface of Pt nanoparticles and the beneficial presence of sodium.

6. Acknowledgements

Financial support from MINECO (Spain) PRI-PIBAR-2011-1349 is acknowledged. The microscopy works have been conducted in the "Laboratorio de Microscopias Avanzadas" at "Instituto de

Nanociencia de Aragon - Universidad de Zaragoza". Authors acknowledge the LMA-INA for offering access to their instruments and expertise.

References

[1] K. Liu, A. Wang, T. Zhang, ACS Catalysis 2 (2012) 1165-1178.
[2] S. Rico-Francés, E.O. Jardim, T.A. Wezendonk, F. Kapteijn, J. Gascon, A. Sepúlveda-Escribano, E.V. Ramos-Fernandez, Applied Catalysis B: Environmental 180 (2016) 169-178.
[3] V. Sebastian, S. Irusta, R. Mallada, J. Santamaría, Applied Catalysis A: General 366 (2009) 242-251.
[4] J. Yan, J.X. Ma, P. Cao, P. Li, Catalysis Letters 93 (2004) 55-60.
[5] C. Wang, L. Zhang, Y. Liu, Applied Catalysis B-Environmental 136 (2013) 48-55.
[6] S.M. Kuznicki, New crystalline titanium silicate molecular sieve zeolite|with defined X=ray powder diffraction pattern, as adsorbent and catalyst, Engelhard Minerals Corp; Engelhard Corp, 1989.
[7] P.V. Snytnikov, V.D. Belyaev, V.A. Sobyanin, Kinetics and Catalysis 48 (2007) 93-102.
[8] J.R. Kitchin, J.K. Nørskov, M.A. Barteau, J.G. Chen, Journal of Chemical Physics 120 (2004) 10240-10246.
[9] S. Zafeiratos, S. Piccinin, D. Teschner, Catalysis Science and Technology 2 (2012) 1787-1801.
[10] W. Yu, M.D. Porosoff, J.G. Chen, Chemical Reviews 112 (2012) 5780-5817.
[11] T. Komatsu, A. Tamura, Journal of Catalysis 258 (2008) 306-314.
[12] C. Wang, B. Li, H. Lin, Y. Yuan, Journal of Power Sources 202 (2012) 200-208.
[13] D.I. Potemkin, E.Y. Filatov, A.V. Zadesenets, P.V. Snytnikov, Y.V. Shubin, V.A. Sobyanin, Chemical Engineering Journal 207–208 (2012) 683-689.
[14] E.Y. Ko, E.D. Park, K.W. Seo, H.C. Lee, D. Lee, S. Kim, Journal of Nanoscience and Nanotechnology 6 (2006) 3567-3571.
[15] C. Kwak, T.J. Park, D.J. Suh, Chemical Engineering Science 60 (2005) 1211-1217.
[16] E.Y. Ko, E.D. Park, H.C. Lee, D. Lee, S. Kim, Angewandte Chemie - International Edition 46 (2007) 734-737.
[17] S. Furukawa, K. Ehara, T. Komatsu, Catalysis Science and Technology 6 (2016) 1642-1650.
[18] H. Xu, Q. Fu, X. Guo, X. Bao, ChemCatChem 4 (2012) 1645-1652.
[19] D.O. Silva, L. Luza, A. Gual, D.L. Baptista, F. Bernardi, M.J.M. Zapata, J. Morais, J. Dupont, Nanoscale 6 (2014) 9085-9092.
[20] H. Huang, Y. Fan, X. Wang, Electrochimica Acta 80 (2012) 118-125.
[21] S. Alayoglu, S.K. Beaumont, F. Zheng, V.V. Pushkarev, H. Zheng, V. Iablokov, Z. Liu, J. Guo, N. Kruse, G.A. Somorjai, Topics in Catalysis 54 (2011) 778-785.
[22] S.C. Tsang, N. Cailuo, W. Oduro, A.T.S. Kong, L. Clifton, K.M.K. Yu, B. Thiebaut, J. Cookson, P. Bishop, Acs Nano 2 (2008) 2547-2553.
[23] X. Du, M. Inokuchi, N. Toshima, Journal of Magnetism and Magnetic Materials 299 (2006) 21-28.
[24] B.M. Faroldi, E.A. Lombardo, L.M. Cornaglia, S. Irusta, Applied Catalysis a-General 417 (2012) 43-52.
[25] L. Lv, F.B. Su, X.S. Zhao, Microporous and Mesoporous Materials 76 (2004) 113-122.
[26] S. Fu, G. Yang, Y. Zhou, H.-B. Pan, C.M. Wai, D. Du, Y. Lin, Rsc Advances 5 (2015) 32685-32689.
[27] G.-H. Wang, J. Hilgert, F.H. Richter, F. Wang, H.-J. Bongard, B. Spliethoff, C. Weidenthaler, F. Schüth, Nat Mater 13 (2014) 293-300.
[28] A.S. Darling, Platinum Metals Reviews 7 (1963) 96-104.
[29] J.-N. Zheng, L.-L. He, C. Chen, A.-J. Wang, K.-F. Ma, J.-J. Feng, Journal of Power Sources 268 (2014) 744-751.
[30] J.R.C. Salgado, E. Antolini, E.R. Gonzalez, Applied Catalysis B: Environmental 57 (2005) 283-290.

[31] B. Li, Z. Yan, Q. Xiao, J. Dai, D. Yang, C. Zhang, M. Cai, J. Ma, Journal of Power Sources 270 (2014) 201-207.
[32] J. Xu, X. Liu, Y. Chen, Y. Zhou, T. Lu, Y. Tang, Journal of Materials Chemistry 22 (2012) 23659-23667.
[33] M. Asteazaran, S. Bengio, W.E. Triaca, A.M. Castro Luna, Journal of Applied Electrochemistry 44 (2014) 1271-1278.
[34] S. Schmid, R. Hausbrand, W. Jaegermann, Thin Solid Films 567 (2014) 8-13.
[35] E. Demirci, M. Öztürk, E. Sınır, U. Ulucan, N. Akdoğan, O. Öztürk, M. Erkovan, Thin Solid Films 550 (2014) 595-601.
[36] X. Yu, W. Yu, H. Li, S.-T. Tu, Y.-F. Han, Applied Catalysis B: Environmental 140–141 (2013) 588-597.
[37] C. Kwak, T.J. Park, D.J. Suh, Applied Catalysis A: General 278 (2005) 181-186.
[38] E.O. Jardim, S. Rico-Frances, F. Coloma, J.A. Anderson, J. Silvestre-Albero, A. Sepulveda-Escribano, Journal of Colloid and Interface Science 443 (2015) 45-55.

Figure captions

Figure 1: a) TEM image of synthesized Pt-Co nanoparticles, b) particle size histogram, c) HAADF-STEM mapping of one particle, d) EDX analysis of particle.

Figure 2: XRD pattern of the synthesized nanoparticles after calcination at 500ºC.

Figure 3: a) Pt4f and b) Co2p core level of PtCo nanoparticles after calcination at 500ºC.

Figure 4: TEM images and particle size distribution of a) and b) 0.35NP/ETS; c) and d) 1.20NP/ETS; e) and f) 1.40NP/ETS.

Figure 5: CO conversion and CO_2 selectivity versus temperature for 1.40 NP/ETS catalysts at different WHSV ($L.h^{-1}.g^{-1}$). Filled symbols correspond to first heating cycle and empty symbols cooling down cycle.

Figure 6: Conversion of CO (filled symbols) and ppm of CO at the outlet (empty symbols) versus temperature for catalysts with different NPs loading: ▼▽ 0.35NP/ETS, ●○0.78 NP/ETS, ▲△1.2 NP/ETS ■□ 1.4 NP/ETS. Empty symbol are for decreasing temperature; b) CO outlet in ppm versus temperature (ºC) WHSV= 30 L/h g.

Figure 7: CO Conversion and selectivity versus time at 75 ºC for 1.40NP/ETS catalyst. WHSV= 30 $L\ h^{-1}g^{-1}$

Figure 1

a)

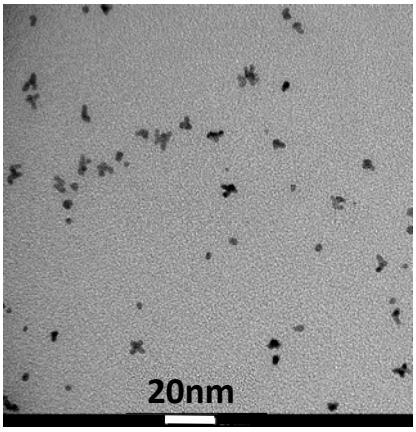

b)

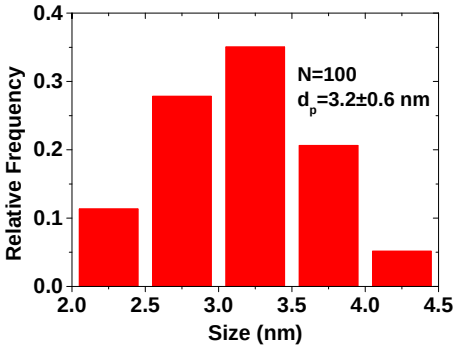

c)

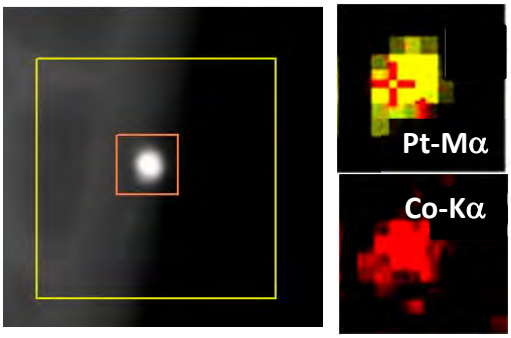

d)

Figure 2

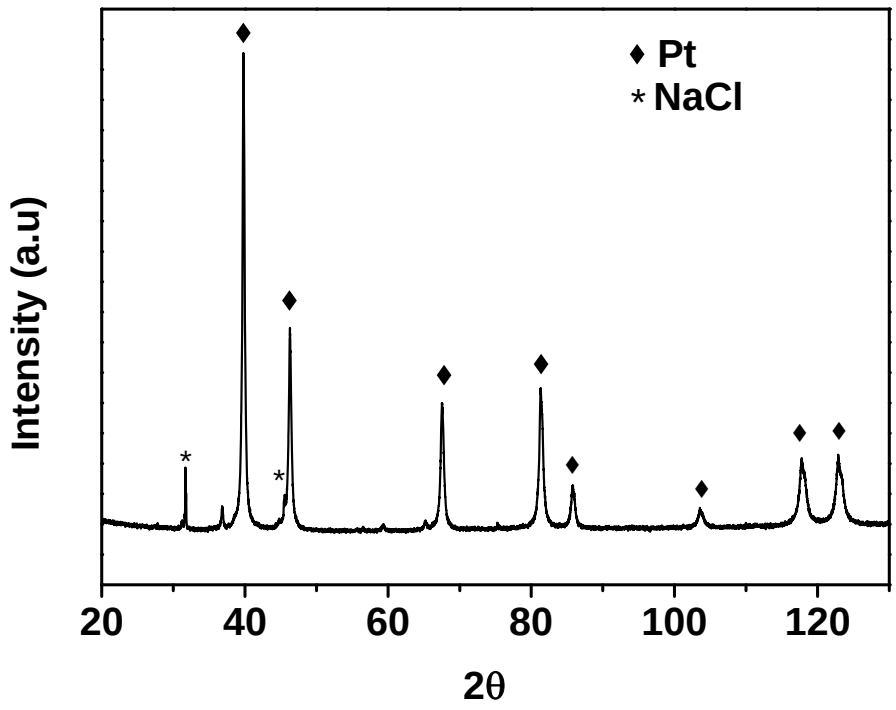

Figure 3

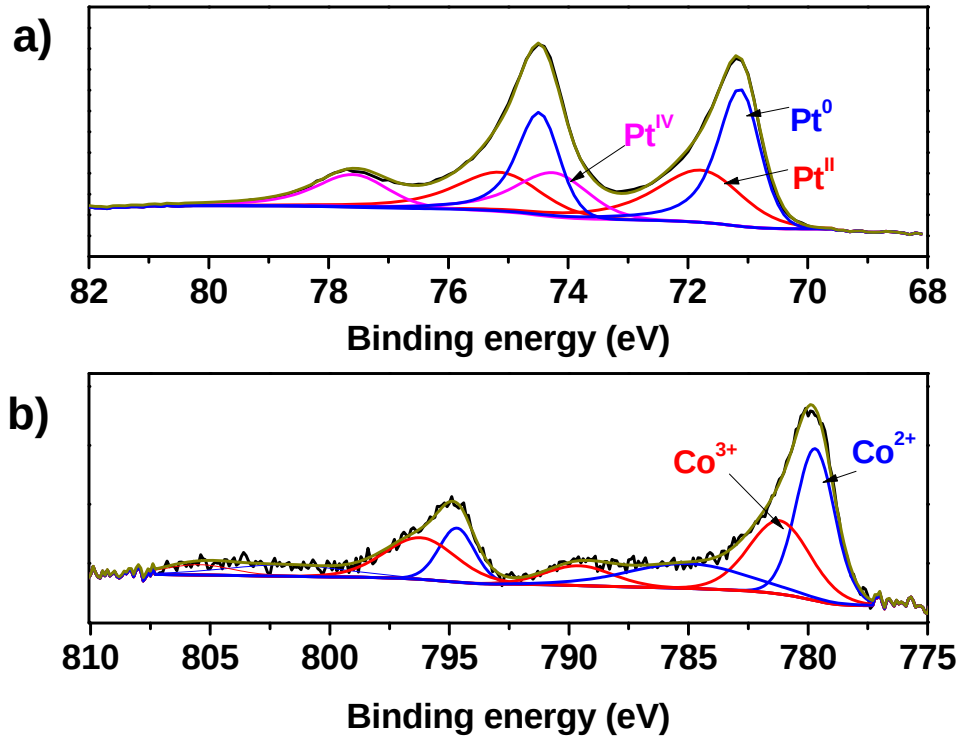
a)
Pt^IV
Pt^0
Pt^II
82
80
78
76
74
72
70
68
Binding energy (eV)
b)
Co^3+
Co^2+
810
805
800
795
790
785
780
775
Binding energy (eV)

Figure 4

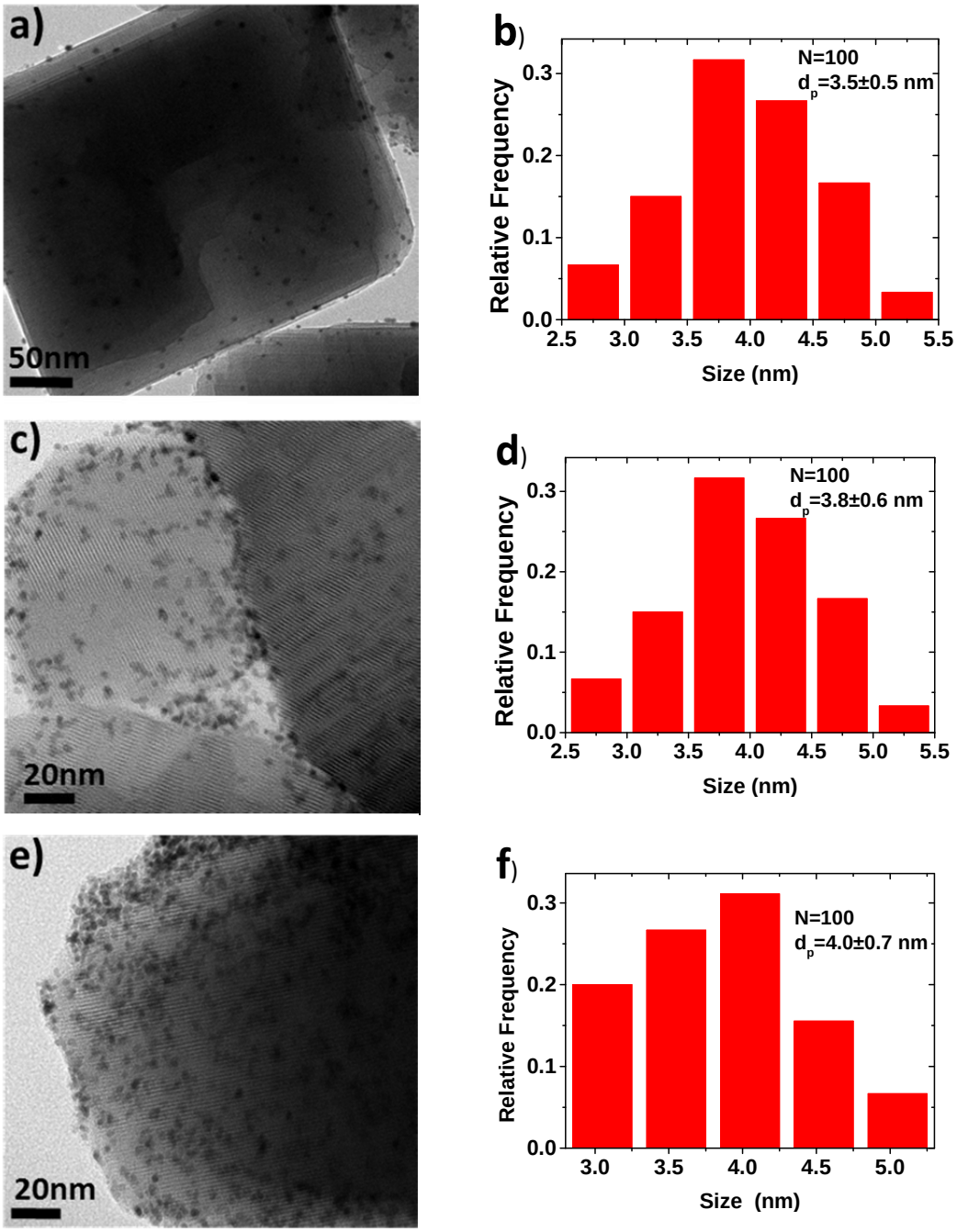
a)
50nm
b)
N=100
d_p=3.5±0.5 nm
Relative Frequency
Size (nm)
c)
20nm
d)
N=100
d_p=3.8±0.6 nm
Relative Frequency
Size (nm)
e)
20nm
f)
N=100
d_p=4.0±0.7 nm
Relative Frequency
Size (nm)

Figure 5

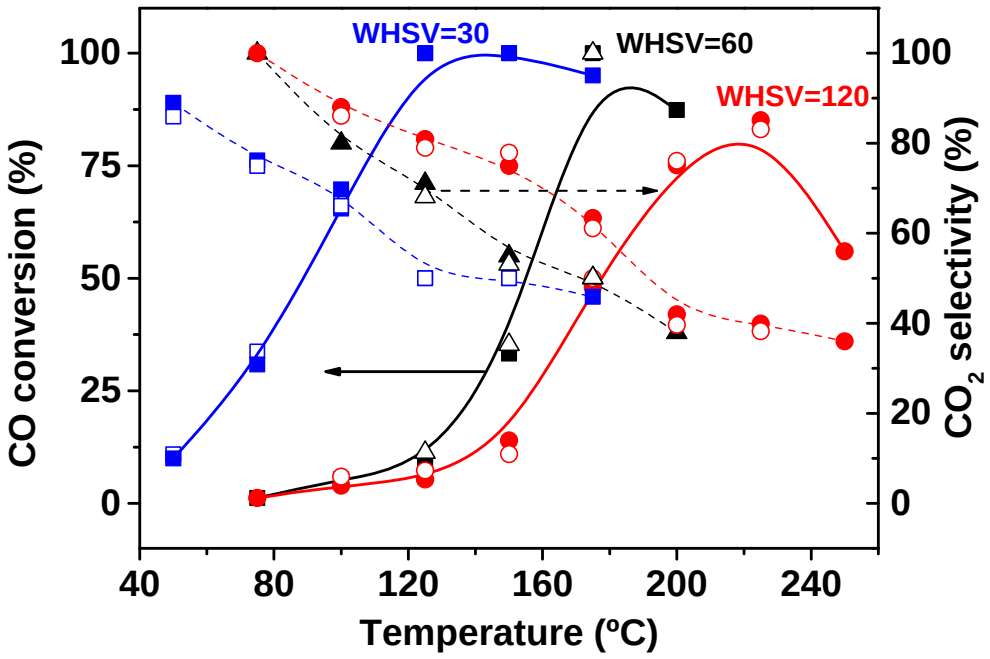
WHSV=30
WHSV=60
WHSV=120
CO conversion (%)
CO_2 selectivity (%)
Temperature (ºC)
100
75
50
25
0
80
60
40
20
40
80
120
160
200
240

Figure 6

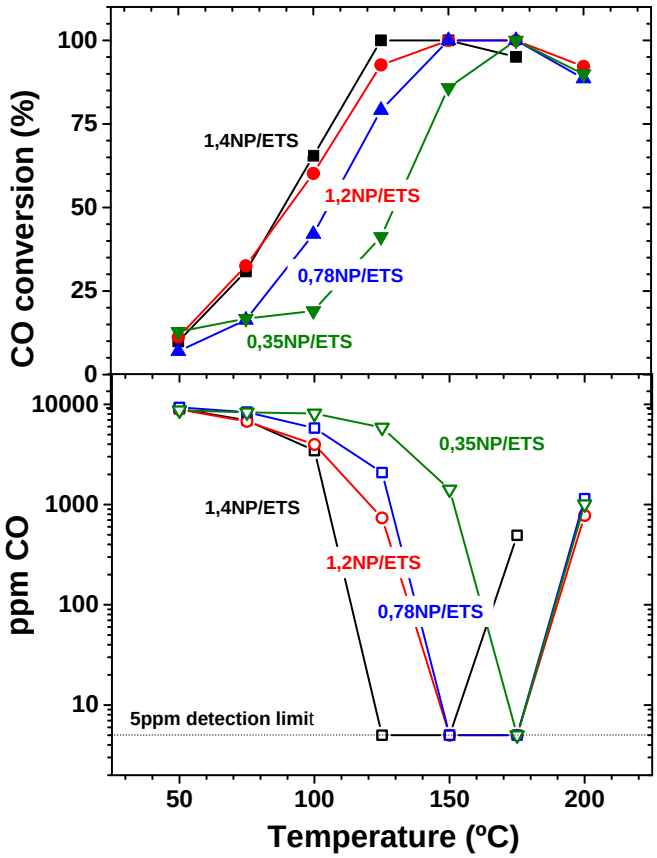
CO conversion (%)
100
75
50
25
0
1,4NP/ETS
1,2NP/ETS
0,78NP/ETS
0,35NP/ETS
ppm CO
10000
1000
100
10
0,35NP/ETS
1,4NP/ETS
1,2NP/ETS
0,78NP/ETS
5ppm detection limit
50
100
150
200
Temperature (ºC)

Figure 7

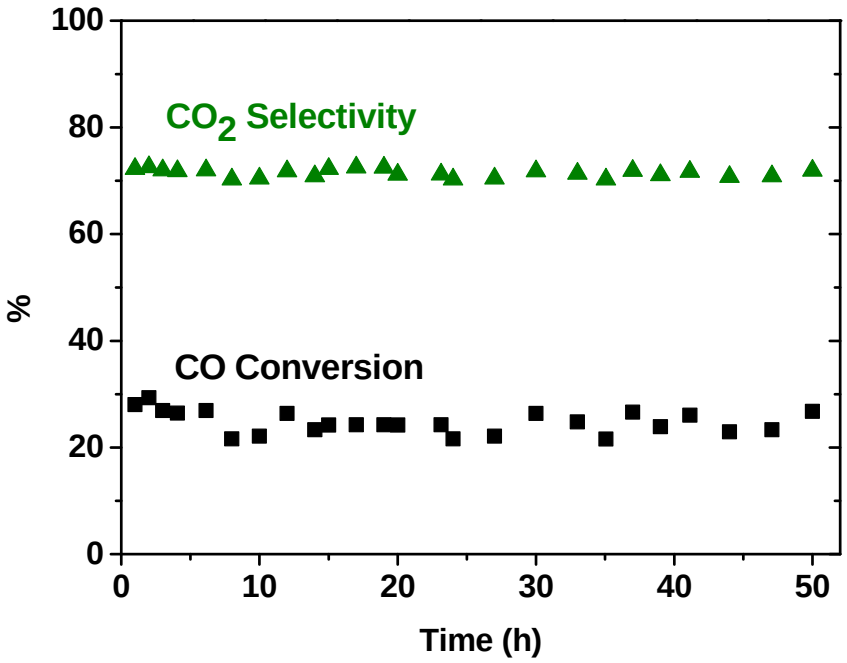
100
80
60
40
20
0
%
CO2 Selectivity
CO Conversion
0
10
20
30
40
50
Time (h)